Multiscale Approach to Damage Analysis of Laminated Composite Structures

D. Ivančević and I. Smojver

Department of Aeronautical Engineering, Faculty of Mechanical Engineering and Naval Architecture, University of Zagreb

I. Lučića 5, HR-10000, Zagreb, Croatia

Abstract: The presented work depicts results of a two-scale approach to the problem of damage and failure prediction on laminated composite structures. Modeling on the micro-level has enabled insight into the underlying physical processes which lead to homogenized properties of the macro-scale material. In this work, micromechanical analysis has been performed by application of the High Fidelity Generalized Method of Cells theory (HFGMC), which is implemented into Abaqus via user material subroutine VUMAT. As result of the HFGMC analysis, micromechanical strain concentration tensors, which relate the strain tensor on the macro-level to the strain tensors of each subcell, have been computed. This enabled calculation of the stress field within the unit cell, based on the constitutive behavior of each subcell. The first stage of modeling damage prediction in composite structures is application of failure criteria in order to account for damage initiation. This work shows results of the application of the most commonly used micromechanical failure criteria applied for unidirectional composites. The micromechanical failure criteria have been compared to the failure criteria applied at lamina (macro) level. The structural model at the macro-scale is a stiffened composite panel, commonly used in aircraft structures.

Keywords: Multiscale analysis, Composite materials, Abaqus/Explicit, High Fidelity Generalized Method of Cells.

List of the most important symbols:

$\mathbf{A}^{(\beta,\gamma)}$ - strain concentration tensor of the β,γ subcell

$\mathbf{C}^{(\beta,\gamma)}$ - elasticity tensor of the β,γ subcell

$\mathbf{C}^{*}$ - equivalent elasticity tensor

h_β, l_γ – subcell dimensions in *2* and *3* directions, respectively

K – unit cell transverse stiffness matrix

L – unit cell axial stiffness matrix

N_β, N_γ – number of subcells in *2* and *3* directions, respectively

V_f - fiber volume fraction

$u_i^{(\beta,\gamma)}$ - displacement field approximation of the β,γ subcell

$u_i'^{(\beta,\gamma)}$ - displacement fluctuation field of the β,γ subcell

$\bar{\boldsymbol{\varepsilon}}^{(\beta,\gamma)}$ - strain tensor of β,γ subcell

$\bar{\boldsymbol{\varepsilon}}$ - macroscopic strain tensor

$\bar{\boldsymbol{\sigma}}^{(\beta,\gamma)}$ - stress tensor of β,γ subcell

1. Introduction

Improvements in the manufacturing technologies resulted in the application of composite materials in primary structural items. A good example of advanced composite application is the wing front spar of the A400M transport aircraft, which is the first application of carbon composites for primary structures on a large transport aircraft wing (Reinforced plastics, 2004). An important contribution to the increasing confidence in composite materials is the improvement of numerical methods used in the virtual testing of composite structures.

The presented work deals with the problem of numerical failure initiation criteria for complex composite structural components. The heterogeneity of composite materials is the source of numerous failure mechanisms which can develop in fiber reinforced composite materials. The most common failure modes are: fiber cracking, fiber pullout, matrix tensile and compressive failure, delamination etc. Apparently, failure of composite structures is a consequence of processes within the heterogeneous composite material.

This fact has led to the idea of performing failure and damage analyses on the constituent level using micromechanical principles, as for example in (Pineda, 2009) and (Sun, 2011). Computing the stresses and strains at the fiber/matrix level enables understanding of the underlying physical processes which lead to damage initiation and progression within the material.

In order to apply the results of the micromechanical analysis in engineering problems, analyses are being performed on several scales. This concept is known as multiscale analysis and is used in many recent research papers on numerical simulation of composite materials, covering a wide range of micromechanical methods (FEM vs. analytical) and engineering problems (metal matrix composites, damage progression etc.) as for example in (Pineda2009) or (Bansal, 2002). The basic idea of the multiscale analysis concept is to transform the solution at the macro-scale to the scale of the fiber and matrix. Failure criteria and effective (macro) material properties are then predicted depending on the solution of the analysis on the micro-scale. Results of the micromechanical analysis, such as material homogenized properties, failure criteria and damage prediction, are afterwards returned to the finite element analysis on the macro-scale.

In this work, computation at the micro-scale has been performed employing a modification of the High Fidelity Generalized Method of Cells (Aboudi, 2003), (Bansal, 2002). The HFGMC model has been included in the Abaqus/Explicit analysis via the user material subroutine VUMAT. The main drawback of the HFGMC, compared to preceding analytical micromechanical models (e.g. Generalized Method of Cells) is the increased computational time of the HFGMC method. As the micromechanical method in this work is being used within explicit finite element analyses, it is obvious that the micromechanical model cannot be used in every time increment, since the analysis in this case would require unacceptably large computation times to obtain final solution.

Therefore, the subject of this work is to compare the most widely used failure criteria on the macro-scale with micromechanical failure criteria found in the literature.

2. Micromechanical model

2.1 High Fidelity Generalized Method of Cells

The micro-scale analysis in this work has been performed using the improved version of the High Fidelity Generalized Method of Cells, after (Bansal, 2002), (Bansal, 2005) and (Bansal 2006). This method belongs to the group of micromechanical models which originate from Aboudi's Method of Cells micromechanical model introduced in (Aboudi, 1987). Aboudi's Method of Cells discretizes a fiber reinforced material by a representative cell, or unit cell (Aboudi 1987). The representative cell is divided into four subcells, of which one represents the fiber while the matrix is represented by the remaining three subcells. An extension of the original model is the Generalized Method of Cells - GMC (Paley, 1992) which allows the composite material unit cell to be represented by an arbitrary number of subcells, enabling modeling of more complex composite materials. This model has been widely used as it enables relatively accurate micro-scale analyses with significantly shorter computational times compared to FEM micromechanical models, as stated in (Gan, 2000). In recent publications, the GMC has been used as a micro-model in multiscale analyses as for example (Pineda 2009). There are several drawbacks which limit the applicability of the GMC model in composite damage prediction analyses as addressed by (Bendarcyk, 2004) and (Bansal, 2006). The most important is the lack of "normal-shear coupling". This means that application of macroscopic normal strains/stresses produces only normal subcell strains/stresses although each subcell is isotropic, transversely orthotropic or orthotropic. Accordingly, macroscopic shear strains/stresses produce only averaged shear subcell strains/stresses. As stated in (Bansal, 2006), this deficiency can potentially produce very inaccurate results in the presence of cracks, disbonds or porosities. A further drawback of the GMC theory is that the displacement field within the unit cell is linear, making it unsuitable for e.g. wave propagation analyses, as stated in (Aboudi, 1987).

The lack of normal-shear coupling and the drawbacks caused by the linear displacement field approximation have been later solved by the High Fidelity Generalized Method of Cells as explained in (Aboudi, 2003) and (Arnold, 2004). HFGMC uses a Legendre type polynomial to approximate the displacement field within the subcell, leading to fundamental differences between the HFGMC and GMC, although they share the same concept of unit cell discretization. Comparison of GMC and HFGMC micromechanical analyses can be found for example in (Bendarcyk, 2004) and (Bansal, 2006).

The micromechanical model in this work is based on the upgraded HFGMC model, which has been initially introduced in (Bansal, 2002). This micromechanical model is in the literature also known as the Finite Volume Direct Averaging Micromechanics (FVDAM), as for example in (Bansal, 2006). The main difference in comparison with the original HFGMC is that it departs from the concept of Generic Cells, significantly reducing the final system of equations by 60%, after (Bansal, 2005).

As the theory of the reconstructed HFGMC micromechanical model is very complex, this work features only some basic equations which are necessary to get an insight into the procedure. More

detailed explanation and discussion on the original and reconstructed HFGMC models can be found in (Aboudi 2003) and (Bansal, 2005).

The unit cell discretization is shown in Figure 1. The model for the unidirectional fiber-reinforced material is based on the assumption that fibers extend in the x_1-direction and are arranged in a doubly periodic array in the x_2 and x_3 directions. The coordinate system used for the HFGMC model corresponds to the material coordinate system of the composite ply, as x_1 is aligned with the fiber direction, x_2 lies in the ply plane and x_3 is perpendicular to the ply plane. The unit cell, having dimensions l x h, is divided into N_β x N_γ subcells, respectively. Each subcell is occupied by either fiber or matrix material.

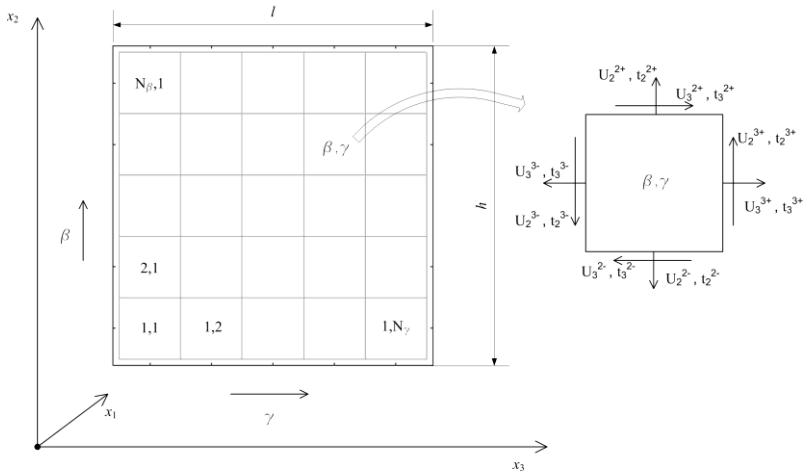

Figure 1. HFGMC model

The aim of the micromechanical analysis is to determine the strain concentration tensor $\mathbf{A}^{(\beta,\gamma)}$, which relates the strain tensor of each subcell $\overline{\boldsymbol{\varepsilon}}^{(\beta,\gamma)}$ to the macroscopic strain field $\overline{\boldsymbol{\varepsilon}}$, after Equation 1.

$$\overline{\boldsymbol{\varepsilon}}^{(\beta,\gamma)} = \mathbf{A}^{(\beta,\gamma)}\overline{\boldsymbol{\varepsilon}} \quad (1)$$

The displacement field within the unit cell is approximated using the same Legendre-type polynomial expansion of the original HFGMC, after (Aboudi, 2003):

$$u_i^{(\beta,\gamma)} = \overline{\varepsilon}_{ij}x_j + W_{i(00)}^{(\beta,\gamma)} + \overline{y}_2^{(\beta)}W_{i(10)}^{(\beta,\gamma)} + y_3^{(\gamma)}W_{i(01)}^{(\beta,\gamma)}$$
$$+\frac{1}{2}\left(3y_2^{(\beta)2} - \frac{h_\beta^2}{4}\right)W_{i(20)}^{(\beta,\gamma)} + \frac{1}{2}\left(3y_3^{(\gamma)2} - \frac{l_\gamma^2}{4}\right)W_{i(02)}^{(\beta,\gamma)}, \; i,j = 1,2,3. \quad (2)$$

The first term on the right side of Equation 2 represents the contribution of the homogenized (averaged) strain, while the rest represents the fluctuating displacement field ($u_i'^{(\beta,\gamma)}$). The W variables in Equation 2 are microvariables which define the fluctuating displacement field within each subcell. These microvariables have to be determined in order to calculate the strain field

within the unit cell. The solution of the micromechanical model begins by defining subcell local stiffness matrices of each subcell. The tractions in the axial (*1*) direction are independent of tractions in the transverse directions (*2* and *3*), enabling separation of the stiffness matrix into axial stiffness matrix **L** and local transverse stiffness matrix **K**. These matrices relate surface averaged tractions *t* of each subcell to the corresponding fluctuating displacements u' at subcell boundaries and macroscopic strains components as defined by Equations 3 and 4, after (Bansal, 2006). The components of vectors *t* and *u* are explained in Figure 1, while the components of stiffness matrices depend on subcell geometry and material elasticity matrix as explained in (Bansal, 2002) and (Bansal, 2005). The *C* values in Equations 3 and 4 are components of the subcell material elasticity matrix.

$$\begin{Bmatrix} \bar{t}_1^{2+} \\ \bar{t}_1^{2-} \\ \bar{t}_1^{3+} \\ \bar{t}_1^{3-} \end{Bmatrix}^{(\beta,\gamma)} = \begin{bmatrix} L_{11} & L_{12} & L_{13} & L_{14} \\ L_{21} & L_{22} & L_{23} & L_{24} \\ L_{31} & L_{32} & L_{33} & L_{34} \\ L_{41} & L_{42} & L_{43} & L_{44} \end{bmatrix}^{(\beta,\gamma)} \begin{Bmatrix} \bar{u}_1'^{2+} \\ \bar{u}_1'^{2-} \\ \bar{u}_1'^{3+} \\ \bar{u}_1'^{3-} \end{Bmatrix}^{(\beta,\gamma)} + 2 \begin{bmatrix} C_{66} & 0 \\ -C_{66} & 0 \\ 0 & C_{55} \\ 0 & -C_{66} \end{bmatrix}^{(\beta,\gamma)} \begin{Bmatrix} \bar{\varepsilon}_{12} \\ \bar{\varepsilon}_{13} \end{Bmatrix}, \quad (3)$$

$$\begin{Bmatrix} \bar{t}_2^{2+} \\ \bar{t}_2^{2-} \\ \bar{t}_3^{2+} \\ \bar{t}_3^{2-} \\ \bar{t}_2^{3+} \\ \bar{t}_2^{3-} \\ \bar{t}_3^{3+} \\ \bar{t}_3^{3-} \end{Bmatrix}^{(\beta,\gamma)} = \begin{bmatrix} K_{11} & K_{12} & 0 & 0 & K_{15} & K_{16} & K_{17} & K_{18} \\ K_{21} & K_{22} & 0 & 0 & K_{24} & K_{25} & K_{26} & K_{27} \\ 0 & 0 & K_{33} & K_{34} & K_{35} & K_{36} & K_{37} & K_{38} \\ 0 & 0 & K_{43} & K_{44} & K_{45} & K_{46} & K_{47} & K_{48} \\ K_{51} & K_{52} & K_{53} & K_{54} & K_{55} & K_{56} & 0 & 0 \\ K_{61} & K_{62} & K_{63} & K_{64} & K_{65} & K_{66} & 0 & 0 \\ K_{71} & K_{72} & K_{73} & K_{74} & 0 & 0 & K_{77} & K_{78} \\ K_{81} & K_{82} & K_{83} & K_{84} & 0 & 0 & K_{87} & K_{88} \end{bmatrix}^{(\beta,\gamma)} \begin{Bmatrix} \bar{u}_2'^{2+} \\ \bar{u}_2'^{2-} \\ \bar{u}_3'^{2+} \\ \bar{u}_3'^{2-} \\ \bar{u}_2'^{3+} \\ \bar{u}_2'^{3-} \\ \bar{u}_3'^{3+} \\ \bar{u}_3'^{3-} \end{Bmatrix}^{(\beta,\gamma)} + \begin{bmatrix} C_{12} & C_{22} & C_{23} & 0 \\ -C_{12} & -C_{22} & -C_{23} & 0 \\ 0 & 0 & 0 & 2C_{44} \\ 0 & 0 & 0 & -C_{44} \\ 0 & 0 & 0 & 2C_{44} \\ 0 & 0 & 0 & -2C_{44} \\ C_{13} & C_{23} & C_{33} & 0 \\ -C_{13} & -C_{23} & -C_{33} & 0 \end{bmatrix}^{(\beta,\gamma)} \begin{Bmatrix} \bar{\varepsilon}_{11} \\ \bar{\varepsilon}_{22} \\ \bar{\varepsilon}_{33} \\ \bar{\varepsilon}_{23} \end{Bmatrix} \quad (4)$$

The global stiffness matrices of the unit cell are assembled after application of traction and continuity conditions at subcell interfaces and periodicity equations at unit cell boundaries as explained in (Bansal, 2002) and (Bansal, 2005). The global system of equations can be decoupled into axial and transverse sets of equations, after (Bansal, 2006). The components of strain tensor in Equations 5 and 6 are referred to homogenized or equivalent deformations of the complete unit cell.

$$\begin{bmatrix} \mathbf{L}_{11} & \mathbf{L}_{12} \\ \mathbf{L}_{21} & \mathbf{L}_{22} \end{bmatrix} \begin{Bmatrix} \begin{bmatrix} \overline{\mathbf{u}}_1'^2 \end{bmatrix} \\ \begin{bmatrix} \overline{\mathbf{u}}_1'^3 \end{bmatrix} \end{Bmatrix} = \begin{bmatrix} \Delta\mathbf{c}_{11} & \mathbf{0} \\ \mathbf{0} & \Delta\mathbf{c}_{22} \end{bmatrix} \begin{Bmatrix} \overline{\varepsilon}_{12} \\ \overline{\varepsilon}_{13} \end{Bmatrix}, \quad (5)$$

$$\begin{bmatrix} \mathbf{K}_{11} & \mathbf{0} & \mathbf{K}_{13} & \mathbf{K}_{14} \\ \mathbf{0} & \mathbf{K}_{22} & \mathbf{K}_{23} & \mathbf{K}_{24} \\ \mathbf{K}_{31} & \mathbf{K}_{32} & \mathbf{K}_{33} & \mathbf{0} \\ \mathbf{K}_{41} & \mathbf{K}_{42} & \mathbf{0} & \mathbf{K}_{44} \end{bmatrix} \begin{Bmatrix} \overline{\mathbf{u}}_2'^2 \\ \overline{\mathbf{u}}_3'^2 \\ \overline{\mathbf{u}}_2'^3 \\ \overline{\mathbf{u}}_3'^3 \end{Bmatrix} = \begin{bmatrix} \Delta\mathbf{C}_{11} & \Delta\mathbf{C}_{12} & \Delta\mathbf{C}_{13} & \mathbf{0} \\ \mathbf{0} & \mathbf{0} & \mathbf{0} & \Delta\mathbf{C}_{24} \\ \mathbf{0} & \mathbf{0} & \mathbf{0} & \Delta\mathbf{C}_{34} \\ \Delta\mathbf{C}_{41} & \Delta\mathbf{C}_{42} & \Delta\mathbf{C}_{43} & \mathbf{0} \end{bmatrix} \begin{Bmatrix} \overline{\varepsilon}_{11} \\ \overline{\varepsilon}_{22} \\ \overline{\varepsilon}_{33} \\ \overline{\varepsilon}_{23} \end{Bmatrix}. \quad (6)$$

The size of the global axial system of equations (Equation 5) is $2N_\beta N_\gamma \times 2N_\beta N_\gamma$, while the transverse system of equations (Equation 6) consists of $4N_\beta N_\gamma \times 4N_\beta N_\gamma$ elements. Global **L** and **K** matrices are assembled from subcell local stiffness matrices as explained in (Bansal, 2006). The submatrices $\Delta\mathbf{c}$ (in Equation 5) and $\Delta\mathbf{C}$ (in Equation 6) contain differences in elastic stiffness elements $C_{ij}^{(\beta,\gamma)}$ between adjacent subcells, after (Bansal, 2005). The displacement vectors in Equations 5 and 6 are comprised of subcell fluctuating interface displacements. The solution of the global system of equations enables calculation of the displacement field within the unit cell. Once the solution of the unit cell displacement field has been obtained, microvariables *W* and strain tensors of each subcell can be computed as explained in (Bansal, 2005). Finally, the stress field within the unit cell is computed based on subcell constitutive model and subcell strain tensors $\overline{\boldsymbol{\varepsilon}}^{(\beta,\gamma)}$

$$\overline{\boldsymbol{\sigma}}^{(\beta,\gamma)} = \mathbf{C}^{(\beta,\gamma)} \overline{\boldsymbol{\varepsilon}}^{(\beta,\gamma)}. \quad (7)$$

The unit cell macroscopic stresses can be obtained by averaging the microscopic stress over the unit cell using equation

$$\overline{\boldsymbol{\sigma}} = \frac{1}{hl} \sum_{\gamma=1}^{N_\gamma} \sum_{\beta=1}^{N_\beta} h_\beta l_\gamma \mathbf{C}^{(\beta,\gamma)} \mathbf{A}^{(\beta,\gamma)} \overline{\boldsymbol{\varepsilon}}, \quad (8)$$

while the equivalent elasticity tensor is calculated using Equation 9

$$\mathbf{C}^* = \frac{1}{hl} \sum_{\gamma=1}^{N_\gamma} \sum_{\beta=1}^{N_\beta} h_\beta l_\gamma \mathbf{C}^{(\beta,\gamma)} \mathbf{A}^{(\beta,\gamma)}. \quad (9)$$

3. Numerical model

3.1 Finite Element Model

The finite element model on which multiscale analyses have been performed represents a composite panel with stringer reinforcements, shown in Figure 2. Such structures are typical structural elements in aeronautical structures. The dimensions and composite layup of the panel are taken from (Degenhardt, 2008). Length and arc length of the panel are 0.78 m and 0.56 m, respectively. The stringers are of a T profile, as shown in Figure 2. The panel skin is made of unidirectional composite plies having a layup $[90/+45/-45/0]_S$, where the orientation of

unidirectional plies is measured with regard to the panel length direction (*z* axis in the Figure 2). The stringers are composed of two sets of $[(+45/-45)_3/0_6]$ laminates, as shown in Figure 2. The thickness of a single ply is 0.125 mm. The finite element model consists of 5270 S4R elements and 5418 nodes, having a total of 32508 degrees of freedom.

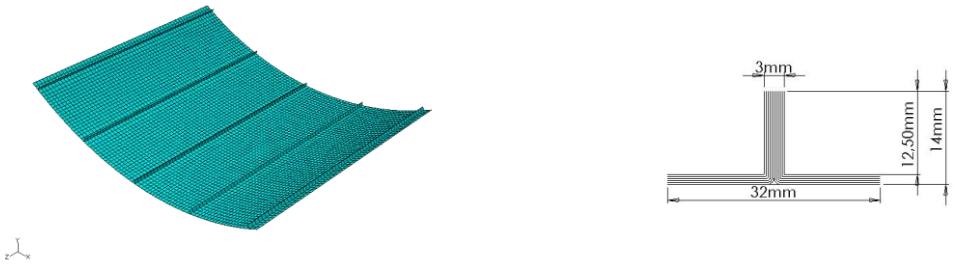

Figure 2. Numerical model and composite layup of the stringer.

The material used for the stringer stiffened panel is carbon fiber reinforced epoxy matrix T300/5208. The constitutive model of the carbon fiber is transversely isotropic, with mechanical properties taken from (Tsai, 1992), (Springer, 2003) and (Hyer, 2009). The matrix is assumed to be isotropic with properties taken from (Tsai, 1992) and (Ehrenstein, 2006). Fiber and matrix properties are listed in Table 1. The homogenized ply material properties have been calculated by HFGMC model, using 30 x 30 subcells to discretize the unit cell and assuming a fiber volume fraction of 70%. Composite ply strengths and other variables needed for calculation of macro-level failure criteria are taken from (Springer, 2003).

Table 1. Fiber and matrix properties

Fiber properties – T300						
$E_1 = 258.57$ GPa	$E_2 = E_3 = 18.69$ GPa	$\nu_{12} = 0.2$	$\nu_{23} = 0.4$	$G_{12} = 19.68$ GPa	$\varepsilon_{1f}^U = 1.4\%$	$\sigma_{ft}^U = 3241$ MPa
Matrix properties – 5208						
$E_1 = 3.4$ GPa	$\nu_{12} = 0.35$	$T_m = 50$ MPa	$C_m = 100$ MPa	$T = 25$ MPa		

Table 2. Calculated lamina properties

Homogenized material properties calculated by HFGMC, 70% fiber volume fraction				
$E_1 = 182.61$ GPa	$E_2 = 11.29$ GPa	$G_{12} = 6.10$ GPa	$\nu_{12} = 0.237$	$\nu_{23} = 0.391$

3.2 Composite Failure Criteria

The micromechanical HFGMC procedure has been included in the Abaqus/Explicit analysis using the user material subroutine VUMAT. Equivalent ply-level properties of the composite material have been calculated by HFGMC and these properties are used to define the linear elastic constitutive behavior of the composite plies. The macro-scale material properties have not been changed during this work, as damage progression has not been included in the analysis. Besides definition of material behavior and micromechanical calculation, the VUMAT subroutine has been used to calculate macro-scale composite failure criteria. The following macroscopic failure criteria have been implemented in the model:

1) Tsai–Wu criterion:

$$F_1\sigma_1 + F_2\sigma_2 + F_6\sigma_6 + F_{11}\sigma_1^2 + F_{22}\sigma_2^2 + F_{66}\sigma_6^2 + 2F_{12}\sigma_1\sigma_2 + 2F_{16}\sigma_1\sigma_6 + 2F_{26}\sigma_2\sigma_6 = 1 \quad (10)$$

2) Tsai-Hill criterion:

$$\frac{\sigma_1^2}{X^2} - \frac{\sigma_1\sigma_2}{X^2} + \frac{\sigma_2^2}{Y^2} + \frac{\tau_{12}^2}{S^2} < 1 \quad (11)$$

3) Hashin failure criteria :

$$\left(\frac{\sigma_{11}}{X_t}\right)^2 + \left(\frac{\tau_{12}}{S_{12}}\right)^2 = 1 \quad \text{- fiber tensile criterion} \quad (12)$$

$$\left(\frac{\sigma_{11}}{X_c}\right)^2 = 1 \quad \text{- fiber compressive criterion} \quad (13)$$

$$\left(\frac{\sigma_{22}}{Y_t}\right)^2 + \left(\frac{\tau_{12}}{S_{12}}\right)^2 = 1 \quad \text{- matrix tensile criterion} \quad (14)$$

$$\left(\frac{\sigma_{22}}{2S_{23}}\right)^2 + \left[\left(\frac{Y_c}{2S_{23}}\right)^2 - 1\right]\frac{\sigma_{22}}{Y_c} + \left(\frac{\tau_{12}}{S_{12}}\right)^2 = 1 \quad \text{- matrix compressive criterion} \quad (15)$$

4) Puck failure criteria:

$\sigma_{f1} = X_{fT}$ for $\sigma_{f1} \geq 0$ and $\sigma_{f1} = -X_{fC}$ for $\sigma_{f1} < 0$ - fiber tensile and compressive failure (16)

$$\sqrt{\left(\frac{\tau_{21}}{R^A_{\perp\parallel}}\right)^2 + \left(1 - \frac{p^{(+)}_{\perp\parallel}}{R^A_{\perp\parallel}}R^{(+)A}_{\perp}\right)\left(\frac{\sigma_2}{R^{(+)A}_{\perp}}\right)^2} + \frac{p^{(+)}_{\perp\parallel}}{R^A_{\perp\parallel}}\sigma_2 = 1 \quad \text{- inter-fiber failure, mode A} \quad (17)$$

$$\sqrt{\left(\frac{\tau_{21}}{R^A_{\perp\parallel}}\right)^2 + 2\left(\frac{p}{R}\right)^2\sigma_2^2} + \left(\frac{p}{R}\right)\sigma_2 = 1 \quad \text{- inter-fiber failure, mode B} \quad (18)$$

$$\left[\left(\frac{\tau_{21}}{2\left(1 + p^{(-)}_{\perp\perp}S_{21}\right)}\right)^2 + \left(\frac{\sigma_2}{Y_C}\right)^2\right]\frac{Y_C}{(-\sigma_2)} + \frac{\sigma_1}{\sigma_{1D}} = 1 \quad \text{- inter-fiber failure, mode C} \quad (19)$$

Discussion on these failure criteria and explanation of symbols used in Equations (10-19) along with standard CFRP ply properties can be found in (Springer, 2003), (Hyer, 2009) and (Puck, 2007). The Tsai-Wu, Tsai-Hill and Hashin criteria are already available in Abaqus, but had to be programmed in VUMAT in order to be able to use results of these criteria in combination with the HFGMC micromechanical analysis.

Micromechanical failure criteria determine failure initiation within the unit cell at the microconstituent level (fiber or matrix). Based on a literature survey on micromechanical composite failure criteria for unidirectional composites, the following criteria have been selected for implementation:

1) 3-D Tsai –Hill criterion to predict matrix failure, after (Pineda, 2009)

$$\frac{\left(\bar{\sigma}_{11}^{(\beta,\gamma)}\right)^2+\left(\bar{\sigma}_{22}^{(\beta,\gamma)}\right)^2+\left(\bar{\sigma}_{33}^{(\beta,\gamma)}\right)^2}{Y^2}+\frac{\bar{\sigma}_{11}^{(\beta,\gamma)}\bar{\sigma}_{22}^{(\beta,\gamma)}+\bar{\sigma}_{11}^{(\beta,\gamma)}\bar{\sigma}_{33}^{(\beta,\gamma)}+\bar{\sigma}_{22}^{(\beta,\gamma)}\bar{\sigma}_{33}^{(\beta,\gamma)}}{Y^2}+\frac{\left(\bar{\sigma}_{12}^{(\beta,\gamma)}\right)^2+\left(\bar{\sigma}_{13}^{(\beta,\gamma)}\right)^2+\left(\bar{\sigma}_{23}^{(\beta,\gamma)}\right)^2}{T^2}=d_m^2, \quad (20)$$

where Y is the matrix transverse strength (tensile or compressive), and T is matrix shear strength. According to (Ehrenstein, 2006), compressive strength of epoxy matrices is approximately twice as high as the tensile strength, while the shear strength is about 50% of the tensile strength value. The assumed epoxy matrix strengths are listed in Table 1.

2) Maximal strain criterion for fiber, used in (Pineda, 2009)

$$\left(\frac{\bar{\varepsilon}_{11}^{(\beta,\gamma)}}{\varepsilon_{ft}^{U}}\right)^2=d_f^2,\ \bar{\varepsilon}_{11}>0, \quad (21)$$

where $\bar{\varepsilon}_{11}^{(\beta,\gamma)}$ are subcell strains in the fiber direction, while ε_{ft}^{U} is the ultimate fiber deformation in fiber direction.

3) Maximal stress for fiber

$$\left(\frac{\bar{\sigma}_{11}^{(\beta,\gamma)}}{\sigma_{ft}^{U}}\right)^2=d_f^2. \quad (22)$$

Similarly to the maximal strain criterion, $\bar{\sigma}_{11}^{(\beta,\gamma)}$ are subcell stresses in the fiber direction while σ_{ft}^{U} is the ultimate fiber tensile stress in the fiber direction.

4) Fiber failure criterion defined in (Sun, 2011)

$$\frac{\bar{\sigma}_{11}^{(\beta,\gamma)2}}{T_f C_f}+\left(\frac{1}{T_f}-\frac{1}{C_f}\right)\bar{\sigma}_{11}^{(\beta,\gamma)}=1, \quad (23)$$

where T_f and C_f are fiber tensile and compressive strengths, respectively.

5) Matrix (inter-fiber) failure, after (Sun, 2011)

$$\frac{\bar{\sigma}_{VM}^{(\beta,\gamma)2}}{T_m C_m}+\left(\frac{1}{T_m}-\frac{1}{C_m}\right)I_1^{(\beta,\gamma)}=1 \quad (24),$$

where $\bar{\sigma}_{VM}^{(\beta,\gamma)}$ is the equivalent stress , while $I_1^{(\beta,\gamma)}$ is the first invariant of the stress tensor of the (β,γ) subcell. Variables T_m and C_m in Equation 24 are matrix tensile and compressive strengths, while T_f and C_f are the corresponding properties of the fiber.

The failure criteria defined by Equations 23 and 24 are parts of the Micromechanics of Failure (MMF) criterion, as stated in (Sun, 2011). The maximal strain and maximal stress criteria for the fiber are straightforward criteria which compare the stress and strain in the fiber with relevant allowables. The 3D Tsai-Hill criterion has been used in (Pineda, 2009) to predict transverse cracking in matrix constituents.

3.3 Micromechanical models

The work described in this paper is currently in the initial phase of implementation of the multiscale computational model, in which the micro-model is used to compare results of macro-scale composite failure criteria with micromechanically calculated failure criteria. At a later stage of this research will the HFGMC model be used to calculate equivalent composite material properties after damage progression. As the HFGMC model is computationally demanding, it should not always be called from the finite element model in order to achieve acceptable computation times. The main purpose of the failure criteria comparison in this work is to select a criterion which will initiate the HFGMC model within the explicit finite element analysis. The time dependent solution of explicit analyses is calculated at a very huge number of time steps, depending on properties of the model and analyzed total time.

Since damage effects are not being evaluated in the current phase of the work, equivalent properties of the composite material have been calculated only at the start of the analysis. These equivalent properties have been used for the macroscopic constitutive equations within the VUMAT subroutine. The calculated properties for the T300/5208 composite ply with 70% fiber volume fraction are listed in Table 2, while the 30 x 30 unit cell used to predict these properties is shown in Figure 3 (left-hand image).

The input variables for the HFGMC model are the current state of macroscopic strain, number of subcells (N_β and N_γ), as well as parameters which define properties of the composite material – fiber and matrix mechanical properties and fiber volume fraction. Each subcell is selected to be a fiber or matrix subcell based on the fiber volume fraction (V_f), number of fibers within the unit cell and position of fiber centers. Figure 3 depicts some unit cells which have been evaluated throughout this research. At the current phase of the methodology development dimensions of all subcells are equal, having dimensions $h_\beta = \frac{h}{N_\beta}$ and $l_\gamma = \frac{l}{N_\gamma}$. This aspect of the model will be improved in order to optimize computational time and enable more flexible unit cell discretization.

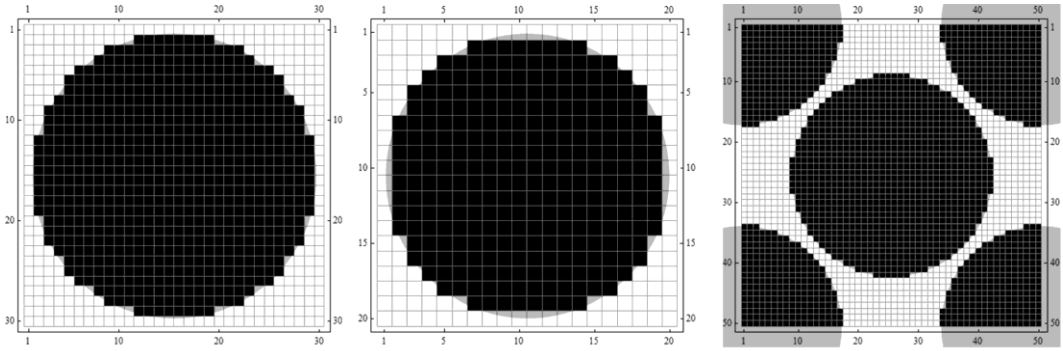

Figure 3. Unit cells used for the HFGMC model.

4. Analysis

As already has been pointed out, this work evaluates the suitability of the HFGMC as a micromechanical model within explicit finite element analyses. Therefore, it has been tested on a relatively simple finite element model, loaded with only static nodal forces. Once the HFGMC subroutine is optimized, it will be used in the impact analyses on complex finite element models.

Boundary conditions have been selected in order to replicate experimental conditions, used on axial testing of similar stiffened panels, as for example in (Degenhardt, 2008). Therefore, nodes at the middle of the panel have restricted degrees of freedom in the axial direction (*z*) and rotational degrees of freedom regarding the *y* direction. Additionally, nodes at the loaded ends of the panel have rigid body constraints, as to simulate the effect of the clamps used to load panels in experiments. The panel has been loaded with an tensile axial force of 255.2 kN (2900 N per node). In order to keep the computational time at a reasonable level, the micromechanical analyses use a 20 x 20 unit cell model with a single fiber in the centre of the unit cell, as depicted on the central image in Figure 3.

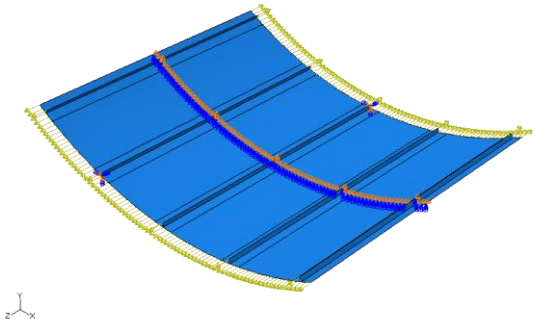

Figure 4. Boundary conditions and loading of the model.

5. Results

In the analyzed load case macroscopically predicted fiber failure criteria reach results below the critical values. Puck's fiber tensile criterion takes the highest fiber failure initiation value (0.45), which is far less than fiber damage onset value. Matrix failure initiation criteria are shown in Figure 5. All failure theories predict matrix damage on a relatively large part of the panel. The Tsai-Hill, Hashin matrix tensile and Puck's Mode A inter-fiber failure criterion predict very similar shapes and sizes of the failed surface, while the Tsai-Wu criterion predicts matrix failure on a significantly larger portion of the panel. This observation is in accordance with conclusions brought by the World Wide Failure Exercise, in which the Tsai-Wu criterion tended to be more conservative compared to more complex failure theories, as stated in (Hinton, 2004). As Puck's failure theory achieved remarkable results in the World Wide Failure Exercise, it has been selected as the criterion which initiates computation of the HFGMC micromechanical model. Consequently, the HFGMC model is activated when the stress state in the finite element analysis of a material point satisfies Equation 17.

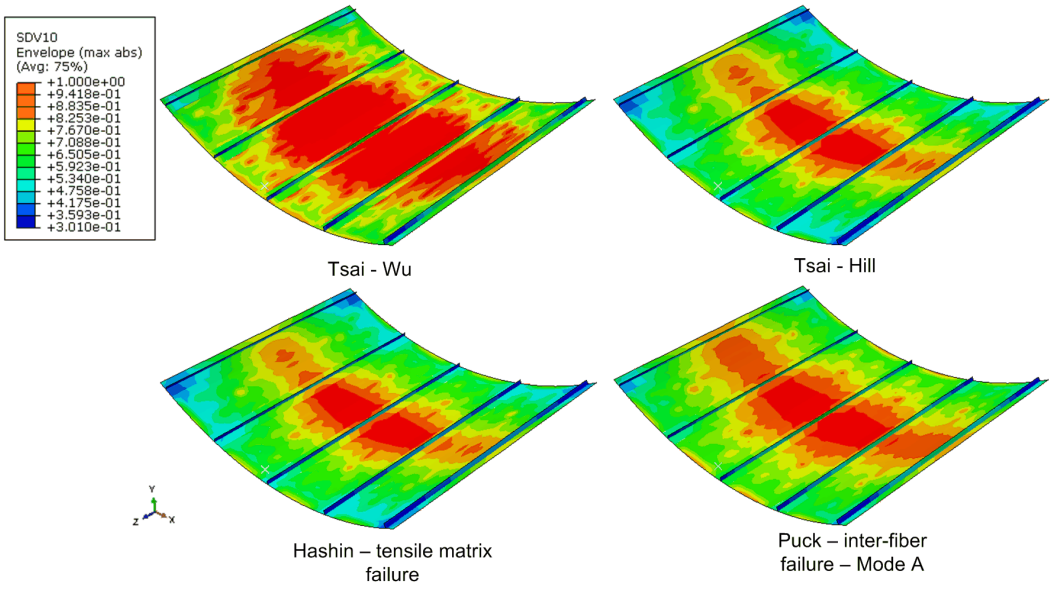

Figure 5. Macroscopic matrix failure criteria, maximal through thickness values are shown.

Micromechaniclly predicted failure theories for matrix failure are shown in Figures 6 and 7. The 3D Tsai-Hill criterion predicts matrix failure indexes between 0.63 and 0.68, as depicted in Figure 6. As all macroscopic failure theories indicate matrix failure, the results of the 3D Tsai-Hill criterion are not consistent with generally accepted macroscopic failure criteria. In order to give insight into the distribution of failure criteria within the unit cell, results of the HFGMC analysis have been shown for particular material point within the finite element model. This material point has been the first to activate calculation on the micro-level with distribution of failure criteria

shown in Figures 6, 7 and 8.The maximal value of the 3D Tsai-Hill criterion has, at that time increment for this particular material point, been 0.655, as shown on the right-hand side image in Figure 6.

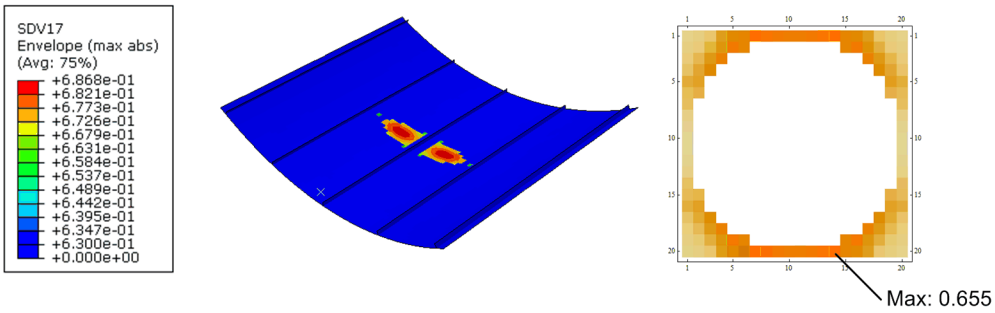

Figure 6. Maximal through thickness values of 3D Tsai Hill micromechanical criterion (left-hand image) and disribution of the criterion within the unit cell

Contrary to the 3D Tsai Hill criterion, the MMF criterion for fiber failure initiation confirms the results of the macroscopic analysis. As shown in Figure 7, all material points predict matrix failure initiation with vaules of the criterion ranging from 1.2 to 1.267. The right-hand side image in Figure 7 shows the distribution of the criterion for the same material point at the same time step as for the one in Figure 6. The distribution of the MMF matrix failure criterion within the unit cell for the examined material point is shown in the right-hand side image of Figure 7. The subcell with maximal value of the criterion is located on a similar position as for the 3D Tsai-Hill criterion in Figure 6. The highest value of the criterion is 1.219.

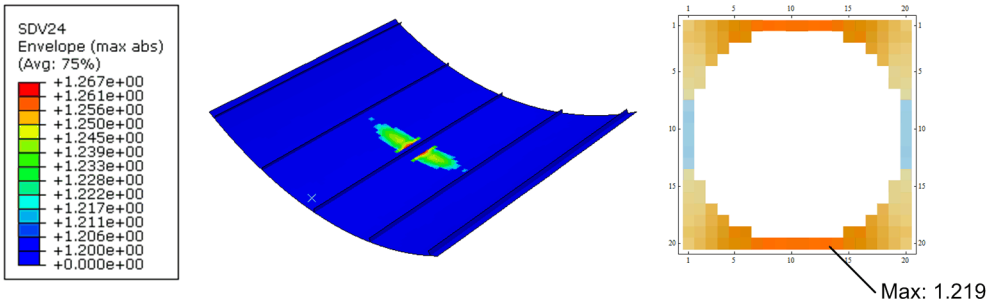

Figure 7. Maximal values of Micromechnics of Failure theory matrix failure criterion in the unit cell.

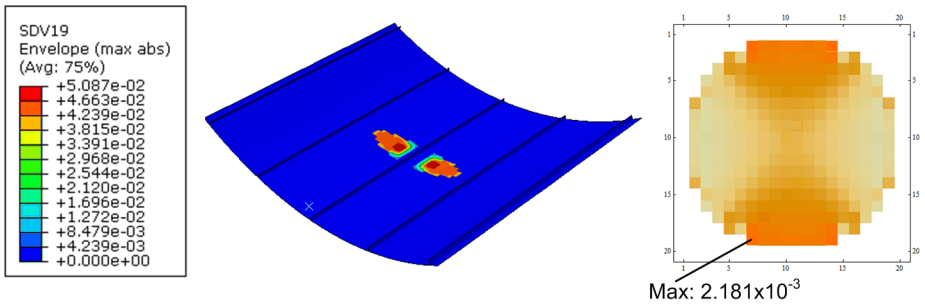

Figure 8. Maximal values of maximal stress criterion for the fiber and distribution of the criterion in the unit cell.

All micromechanically calculated fiber failure criteria predict significantly lower values compared to macro-level failure criteria associated with fiber failure. Maximal through thickness values of the maximal stress criterion are shown in Figure 8. The distribution of the criterion within the unit cell for the evaluated material point is shown in the right-hand side image of Figure 8.

6. Conclusion

The work presented in this paper illustrates results of the initial phase of the HFGMC micromechanical model implementation into Abaqus/Explicit. Concerning the available computational resources, the HFGMC micromechanical model is not suitable for computation at all time increments of all material points during an explicit finite element analysis, as such an application of the model would lead to unacceptably high computational times. In the ongoing research, the HFGMC will be employed to predict equivalent composite properties after damage initiation. Therefore, the basic idea of the current research is to select a criterion which will initiate computation on the micro-level. Comparison of macroscopically predicted composite failure criteria revealed Puck's mode A inter-fiber failure criteria as the best choice for HFGMC initiation.

As indicated in Section 5, the 3D Tsai-Hill criterion and the MMF matrix failure criterion show significant discrepancies when indicating whether the matrix has failed or not. This result could be strongly influenced by the accuracy of estimation of strength values for the epoxy matrix. These material properties have been estimated according to guidelines given in (Ehrenstein, 2006). The fiber failure criteria on the micro-level predict that fiber failure does not occur in the analyzed load case, which is in accordance with the macroscopically predicted fiber failure criteria.

As the multiscale analysis procedure presented in this work is still in the development and testing phase, this work gives only an overview of the applied model and therefore comparison with experimental results has not been carried out. The presented results and the research currently in progress are aimed at application of this methodology in other areas of damage analysis in composite aeronautical structures, such as effects of blast loads, high velocity /high strain phenomena and others, where Abaqus/Explicit will be employed.

7. References

1. Aboudi, J, A., "Closed Form Constitutive Equations for Metal Matrix Composites," International Journal of Engineering Science, vol. 25, no. 9, pp.1229-1240, 1987.
2. Aboudi, J., M.-J. Pindera and S. M. Arnold, "Higher-Order Theory for Periodic Multiphase Materials with Inelastic Phases," International Journal of Plasticity, no. 19, pp. 805-847, 2003.
3. Arnold, S. M., B. Bednarcyk, and J. Aboudi, "Comparison of the Computational Efficiency of the Original Versus Reformulated High-Fidelity Generalized Method of Cells," NASA/TM – 2004-213438, 2004.
4. Bansal, Y. and M.-J. Pindera, "Efficient Reformulation of the Thermoelastic Higher-Order Theory for FGMs," NASA/CR – 2002 – 211909, 2002.
5. Bansal, Y. and M.-J. Pindera, "A Second Look at the Higher-Order Theory for Periodic Multiphase Materials," Journal of Applied Mechanics, no. 72, pp. 177-195, 2005.
6. Bansal, Y. and M.-J. Pindera, "Finite-Volume Direct Averaging Micromechanics of Heterogeneous Materials with Elastic-Plastic Phases," International Journal of Plasticity, no. 22, pp. 775-825, 2006.
7. Degenhardt, R., A. Kling, K. Rohwer, A. C. Orifici and R. S. Thomson, "Design and Analysis of Stiffened Composite Panels including Post-Buckling and Collapse," Computers and Structures, no. 86, pp. 919-929, 2008.
8. Ehrenstein, G. W., "Faserverbund-Kunststoffe," Carl Hanser Verlag München Wien, 2006.
9. Hinton M. J., A. S. Kaddour, and P. D. Soden, "A Further Assessment of the Predictive Capabilities of Current Failure Theories for Composite Laminates: Comparison with Experimental Evidence," Composites Science and Technology, no. 64., pp. 549-588, 2004.
10. Hyer, M. W., "Stress Analysis of Fiber-Reinforced Composite Materials," DEStech Publications, 2009.
11. Paley, M. and J. Aboudi, "Micromechanical Analysis of Composites by the Generalized Cells Model," Mechanics of Materials, no. 14, pp. 127-139, 1992.
12. Pineda, E. J., A. M. Waas and B. A. Bednarcyk, "Multiscale Model for Progressive Damage and Failure of Laminated Composites Using an Explicit Finite Element Method," 50th AIAA/ASME/ASCE/AHS/ASC Structures, Structural Dynamics, and Materials Conference, 2009.
13. Puck, A. and M. Mannigel, "Physically Based Non-Linear Stress-Strain Relations for the Inter-Fibre Fracture Analysis of FRP Laminates," Composites Science and Technology, no. 67, pp. 1955-1964, 2007.
14. "GKN Wins A400M Wing Spar Contract," Reinforced Plastics, 2004.
15. Springer, G.S and Kollar, L. P., "Mechanics of Composite Structures," Cambridge University Press, 2003.
16. Sun, X. S., V. B. C. Tan, and T. E. Tay, "Micromechanics-Based Progressive Failure Analysis of Fibre-Reinforced Composites with Non-Iterative Element-Failure Method," Computers and Structures, no. 89, pp. 1103-1116, 2011.
17. Tsai, S. W. "Theory of Composites Design," Think Composites, 1992.